

Collective non-Hermitian skin effect: Point-gap topology and the doublon-holon excitations in non-reciprocal many-body systems

Beom Hyun Kim,¹ Jae-Ho Han,¹ and Moon Jip Park^{2,*}

¹*Center for Theoretical Physics of Complex Systems,
Institute for Basic Science, Daejeon 34126, Republic of Korea*

²*Department of Physics, Hanyang University, Seoul 04763, Republic of Korea*
(Dated: November 23, 2023)

Open quantum systems provide a plethora of exotic topological phases of matter that has no Hermitian counterpart. Non-Hermitian skin effect, macroscopic collapse of bulk states to the boundary, has been extensively studied in various experimental platforms. However, it remains an open question whether such topological phases persist in the presence of many-body interactions. Notably, previous studies have shown that the Pauli exclusion principle suppresses the skin effect. In this study, we present a compelling counterexample by demonstrating the presence of the skin effect in doublon-holon excitations. While the ground state of the spin-half Hatano-Nelson model shows no skin effect, the doublon-holon pairs, as its collective excitations, display the many-body skin effect even in strong coupling limit. We rigorously establish the robustness of this effect by revealing a bulk-boundary correspondence mediated by the point gap topology within the many-body energy spectrum. Our findings underscore the existence of non-Hermitian topological phases in collective excitations of many-body interacting systems.

Introduction– Dissipation is a ubiquitously observed phenomenon in many physical systems. In quantum systems, the presence of the dissipation leads to complex-valued eigenenergies, which mark the onset of non-Hermitian quantum mechanics. Non-reciprocal interactions, which are typical in out-of-equilibrium phenomena, are another important source of non-Hermiticity. The broad applicability of non-Hermitian quantum mechanics has attracted considerable interest in various fields of physics including physics, such as high-energy [1–4], optics [5–10], cold atoms [11–15], and condensed matter systems [16–23].

Recent progress in the field of non-Hermitian topological phases has shown great promise in discovering new types of topological phases [24–36]. The non-Hermitian skin effect (NHSE), which exhibits the macroscopic collapse of the eigenstates to the boundary, is the representative example [37–52]. However, the fate of the NHSE in the presence of the many-body interaction is still elusive. Previous studies reveal that the NHSE can be fragile against many-body effects [53–58]. For instance, in the half-filled interacting Hatano-Nelson model, the macroscopic accumulation of charge at the boundary is generally prohibited by the Pauli exclusion principle.

In this work, we firstly establish the case that the NHSE robustly exists as a form of collective excitations. Unlike spinless models, the antiferromagnetic Mott insulator ground states of the spin-half Hatano-Nelson model harbor the doublon-holon pairs as well-defined collective excitations even in strong interacting limits. While the ground state does not exhibit the NHSE, we

show that the excited states with the doublon-holon pairs show the helical skin effect, where the doublon and the holon exhibit the counterpropagating accumulations of the charge at the opposite boundaries. We formally establish this exotic collective NHSE by illustrating bulk-boundary correspondence mediated by point-gap topology in the many-body energy spectra.

Lattice Model and Symmetries– We consider the one-dimensional interacting Hatano-Nelson model of spin-half fermions, which is described by the following Hamiltonian:

$$H = -t \sum_{l=0}^{L-2} \sum_{\sigma} \left(e^A c_{l+1,\sigma}^{\dagger} c_{l,\sigma} + e^{-A} c_{l,\sigma}^{\dagger} c_{l+1,\sigma} \right) + U \sum_{l=0}^{L-1} n_{l,\uparrow} n_{l,\downarrow} + H_B, \quad (1)$$

Here, $c_{l,\sigma}^{\dagger}$ ($c_{l,\sigma}$) are the fermion creation (annihilation) operators with spin σ ($=\uparrow, \downarrow$) at the l -th site, $n_{l,\sigma} = c_{l,\sigma}^{\dagger} c_{l,\sigma}$ is the number operator, and U is the strength of on-site Coulomb repulsion strength between doubly occupied fermions. The lattice size is denoted by L and A represents the imaginary vector potential that introduces non-reciprocal hopping [16, 17]. The boundary term H_B accounts for the hopping Hamiltonian between the end sites. For example, in open boundary conditions (OBC), H_B is 0, while $H_B = -t \left(e^A c_{0,\sigma}^{\dagger} c_{L-1,\sigma} + e^{-A} c_{L-1,\sigma}^{\dagger} c_{0,\sigma} \right)$ for periodic boundary conditions (PBC). In general twisted boundary conditions (TBC), H_B takes a form, $-t \left(e^{A+i\phi} c_{0,\sigma}^{\dagger} c_{L-1,\sigma} + e^{-A-i\phi} c_{L-1,\sigma}^{\dagger} c_{0,\sigma} \right)$, where ϕ represents the $U(1)$ -gauge (magnetic) flux.

The symmetry of the Hamiltonian depends on both boundary conditions and the presence of the many-body

* moonjipark@hanyang.ac.kr

interactions. In the non-interacting limit ($U = 0$), the Hamiltonian under PBC and TBC satisfies the normality ($HH^\dagger = H^\dagger H$), which allows to have orthonormalized eigenstates. The corresponding eigenvalue spectra in PBC can form a closed contour with non-trivial point gap topology. In the corresponding OBC, the normality is lost. Instead, there exists the similarity transformation with the invertible operation S that satisfies $H_{A=0} = S^{-1}HS$, where $H_{A=0}$ is the Hermitian Hamiltonian without the imaginary gauge flux A (see Supplement Materials (SM) [59]). As a result, all eigenvalues exhibit the purely real numbers [60]. The collapse of the eigenenergies to the real axis manifests as the NHSE.

Even in the finite many-body interaction ($U \neq 0$), we can find the similarity transformation S such that $H_{A=0} = S^{-1}HS$ under OBC, resulting the purely real eigenvalues. However, the normality is broken regardless of the boundary condition due to the inclusion of U . Moreover, H for PBC and TBC becomes \mathcal{PT} -pseudo-Hermitian, where \mathcal{P} and \mathcal{T} are inversion and time-reversal operators, respectively [59]. Consequently, the eigenvalues are either real or occur in complex-conjugate pairs [61].

Non-Hermitian skin effect— We represent the many-body eigenstates using orthonormal basis states: $|\Psi_n\rangle = \prod_{j=1}^N c_{l_{nj}, \sigma_{nj}}^\dagger |vac\rangle$, where l_{nj} and σ_{nj} denote the site index and spin state of the j th fermion for the n th basis state, respectively. $|vac\rangle$ represents the vacuum state, and N is the total number of fermions. The similarity transformation S such that $H_{A=0} = S^{-1}HS$ under OBC is given as following [59]:

$$S = \sum_n e^{A \sum_{j=1}^N l_{nj}} |\Psi_n\rangle \langle \Psi_n|. \quad (2)$$

The non-orthonormal factor $C_n(A) = e^{A \sum_{j=1}^N l_{nj}}$ causes coefficients of eigenstates to vary exponentially with A , playing a crucial role in determining the NHSE in many-

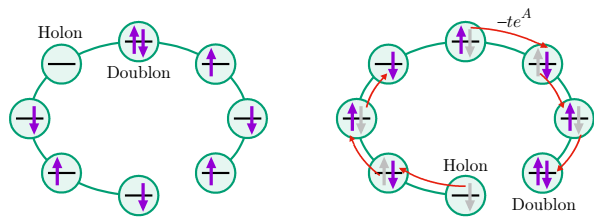


FIG. 1. Schematic diagrams of the motion of the doublon (doubly occupied site) and holon (empty site) in the present of non-reciprocal hopping. As illustrated on the right panel, non-reciprocal hopping, denoted by red arrows, results in the rightward (leftward) movement of doublons (holons). The gray arrows represent the initial positions of fermion spins prior to hopping. Under OBC, doublon and holon become localized at opposite edges of one dimensional chain. This segregation in localized doublon and holon is responsible for the NHSE.

body systems [56, 59, 62].

With respect to the half-filled ground state ($N = L$), $C_n(A)$ can vary depending on the distribution of doubly occupied sites, called doublons, and empty sites, referred to as holons [59]. Explicitly, let N_d be the total number of doublon-holon pairs. $C_n(A)$ is expressed as

$$C_n(A) = e^{A \frac{L(L-1)}{2}} e^{A \sum_{j=1}^{N_d} (l_{nj}^d - l_{nj}^h)}, \quad (3)$$

where l_{nj}^d and l_{nj}^h denote the site indices of the j th doublon and holon for the n th basis state $|\Psi_n\rangle$, respectively. For states with no doublon-holon pair ($N_d = 0$), $C_n(A)$ reaches its minimum with a constant value of $e^{A \frac{L(L-1)}{2}}$. These states exhibit little influence from the NHSE. On the other hand, for states with finite doublon-holon pairs, $C_n(A)$ grows exponentially as the strength of A increases. The larger the segregation between doublons and holons, quantified by $\sum_{j=1}^{N_d} (l_{nj}^d - l_{nj}^h)$, the larger $C_n(A)$ becomes. Hence, the NHSE in the half-filled case is characterized by the segregation of doublons and holes.

The relation between the NHSE and the segregation of doublons and holons can be explained by considering the non-reciprocal mobility of these particles. As illustrated in Fig. 1, let us imagine that a doublon-holon pair forms between neighboring sites in a half-filled state. When a positive $A > 0$ is present, the hopping strength from the left site to the right site becomes larger than the opposite direction. This enhances the fermion on the left side of the holon site to preferentially occupy that site, leading to the holon's movement to the right. In contrast, one of the fermions occupying the doublon site is more likely to hop to the next site on the right, resulting in the doublon's movement to the left. As a result, doublons and holons become separated and localized at opposite boundary sites under OBC. Conversely, for PBC, doublons and holons merge again. This distinctive non-reciprocal behavior of doublons and holons underpins the emergence of the NHSE in the half-filled case.

In many-body systems governed by the Pauli exclusion principle, one effective approach to demonstrate the NHSE is by quantifying the asymmetry in the distribution of number density along an open-boundary chain [56]. To achieve this, we calculate the number density distribution of the right eigenstates using the formula: $n_E^R(l) = \langle \Psi_E^R | \sum_{\sigma} c_{l,\sigma}^\dagger c_{l,\sigma} | \Psi_E^R \rangle / \langle \Psi_E^R | \Psi_E^R \rangle$. This distribution's asymmetry results in the number imbalance of fermions located at below $L/2$ ($0 \leq l < L/2$) and above $L/2$ ($L/2 \leq l < L$) sites. We can quantify this imbalance with the following formula:

$$\mathcal{I}_E^R = \sum_{L/2 \leq l < L} n_E^R(l) - \sum_{0 \leq l < L/2} n_E^R(l). \quad (4)$$

The occurrence of non-zero values for \mathcal{I}_E^R is a distinctive indicator of the many-body NHSE, as detected within right eigenstates.

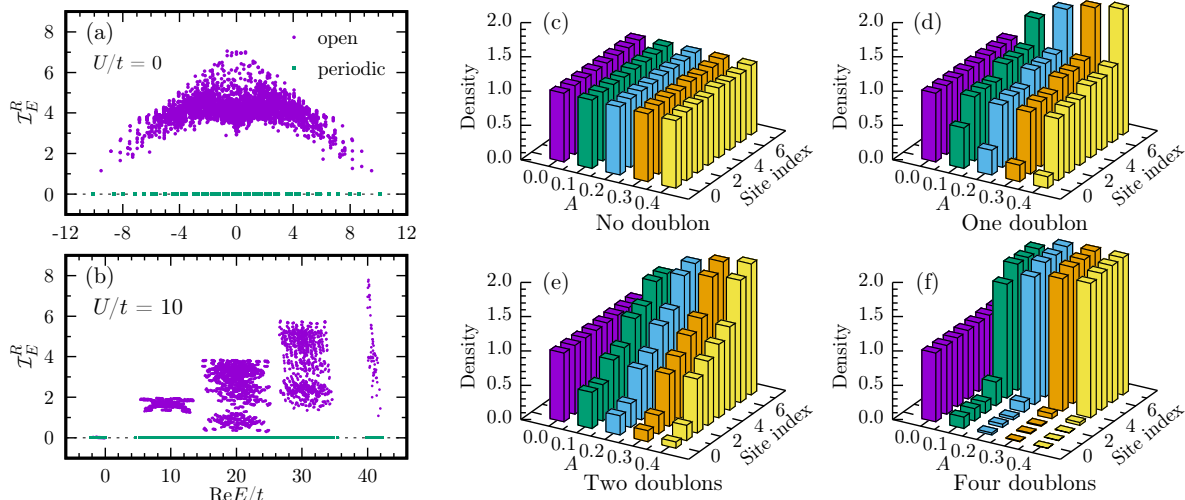


FIG. 2. The number density imbalance in the half-filled Hatano-Nelson model of spin-half fermions ($A = 0.3$) under both OBC and PBC when (a) $U/t = 0$ and (b) $U/t = 10$. The imbalance \mathcal{I}_E^R is calculated by $\sum_{L/2 \leq l < L} n_E^R(l) - \sum_{0 \leq l < L/2} n_E^R(l)$, where $n_E^R(l)$ is the number density of right eigenvalues at the l th site. (c)–(f) the number density distributions as a function of imaginary gauge potential A for specific right eigenstates, where no, one, two, and four doublon-holon pairs play a dominant role for OBC. All results are obtained for a lattice size of eight ($L = 8$).

Fig. 2 exhibits the calculated number density distribution, clearly showing that the asymmetric nature is present under OBC for both non-interacting ($U = 0$) and interacting ($U \neq 0$) cases. The corresponding finite values of imbalance \mathcal{I}_E^R affirm this. However, the situation differs for PBC, where \mathcal{I}_E^R consistently equals zero. These results depict the NHSE in non-reciprocal many-body systems.

In the non-interacting case ($U = 0$), \mathcal{I}_E^R exhibits an arch-like pattern, ranging from about 1 to roughly 7 for $L = 8$. In contrast, strong interactions ($U = 10t$) yield a stair-like \mathcal{I}_E^R pattern. This can be understood by the spectral properties of the Mott insulating region. With a substantial Coulomb repulsion (U), eigenvalues mainly depend on U strength, leading to sizable separations related to the number of doublon-holon pairs (N_d). When N_d -dominated states prevail in the eigenstates, \mathcal{I}_E^R attains a maximum value of around $2N_d$ for OBC. This feature is well captured by Fig. 2(b).

Furthermore, the non-reciprocal hopping causes opposing doublon and holon propagation. Initially, they gather at opposing boundaries for finite A . The Pauli exclusion principle then drives further accumulation near by initial sites. This pattern is visually evident in the calculated number density distributions, depicted in Figs. 2(c)–(f). Consequently, we deduce that the NHSE in the many-body system can be understood through the segregation of doublons and holons within the half-filled Hatano-Nelson model of spin-half fermions.

Complex eigenspectrum and point-gap topology— As shown in Fig. 3(a), for PBC, the eigenvalues of the Hamiltonian can take either on purely real values or

form complex conjugate pairs. This originates from the pseudo-Hermiticity of the Hamiltonian. To gain a deeper understanding of the spectral properties, we analyze how eigenvalues change with the gauge flux ϕ under TBC. Figs. 3(b) and (c) provide the trajectory of complex eigenvalues when the real part of the eigenvalue lies between $4t$ and $14t$ (one doublon-holon sector) and between $39t$ and $43t$ (four doublon-holon sector), respectively.

As ϕ changes from 0 to 2π , complex eigenvalues undergo rotations in the complex plane, effectively tracing closed paths alongside other eigenvalues. This rotation ultimately results in non-zero integer winding numbers, which can be calculated using the formula:

$$W(E_p) = \oint_0^{2\pi} \frac{d\phi}{2\pi i} \frac{d}{d\phi} \log \det [H(\phi) - E_p], \quad (5)$$

Here, E_p stands for the point gap of the complex energy [54, 55]. This behavior highlights the intriguing topological aspects inherent to the system.

In the non-interacting case, all complex eigenvalues wind around the origin ($E = 0$). It implies that the point gap is straightforwardly identified at the center of the complex plane (see SM [59]). However, in the interacting case, as seen in Fig. 3(b) and (c), multiple point gaps are not isolated but emerge near the energy center of doublon-holon sectors. This multiplicity of point gaps defines the non-Hermitian topology of non-reciprocal many-body systems.

In the strong interaction limit, the many-body NHSE does not emerge for eigenstates mainly contributed to states with no doublon-holon pair in the half-filled case.

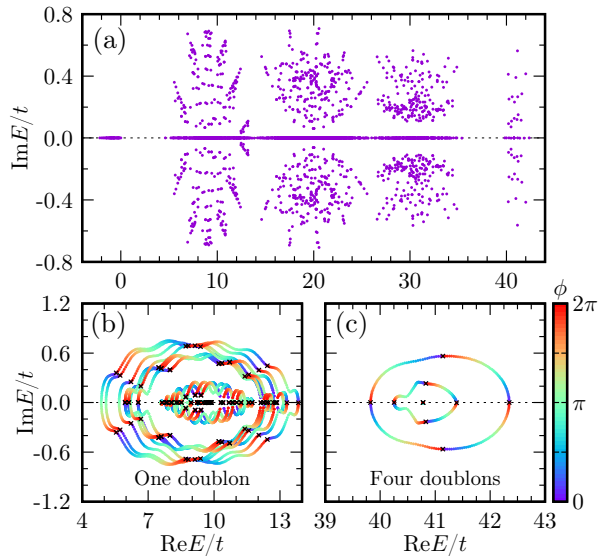


FIG. 3. (a) Eigenvalue spectrum in the half-filled Hatano-Nelson model of spin-half fermions with $U/t = 10$ and $A = 0.3$. Notably, even under strong interaction limit, complex eigenvalues remain robust within finite doubton-holon sectors. Spectral evolution of eigenvalues as functions of the gauge flux ϕ for TBC in (b) one and (c) four doubton-holon sectors. For simplicity, only eigenvalues corresponding to the crystal momentum $k = 0$ and the z -component of the total spin $S_z = 0$ are presented in (b) and (c) by utilizing the translation symmetry and S_z conservation (see SM [59]). Cross points indicate eigenvalues at $\phi = 0$. These spectral data effectively depict the point-gap topology of complex eigenvalues. All results are obtained for a lattice size of eight ($L = 8$).

Correspondently, eigenvalues below zero remain purely real even for PBC. In the second-order perturbation limit, the effective Hamiltonian in no doubton-holon sector is described with the Heisenberg interaction, given as $H_{\text{eff}} = J \sum_l \mathbf{S}_l \cdot \mathbf{S}_{l+1}$ [63]. The magnetic interaction among neighboring spins (J) is determined by virtual hopping processes, in which fermions hop forth and back neighboring sites. J is expected to be robust as $J = \frac{4t^2 e^A e^{-A}}{U} = \frac{4t^2}{U}$. Therefore, the real eigenvalues are stabilized for no doubton-holon sector in the strong interaction limit (see SM [59]).

When the total number of doubton-holon pairs are $L/2$, $L/2$ number of doublons and holons occupy all lattice sites. In this situation, we can construct the effective model using attracted half-filled hard-core bosons with non-reciprocal hopping in the second-order perturbation limit. The effective attracted interaction, hopping strength, and effective imaginary gauge are estimated by $U_{\text{eff}} = -\frac{4t^2}{U}$, $t_{\text{eff}} = \frac{2t^2}{U}$, and $A_{\text{eff}} = 2A$, respectively (see SM [59]). Since $|U_{\text{eff}}|/t_{\text{eff}} = 2$ is much smaller than U/t and A_{eff} is the twice of A , the robustness of complex eigenvalues can be maintained even when U exceeds t much largely.

Topological transition and exceptional points– Due to

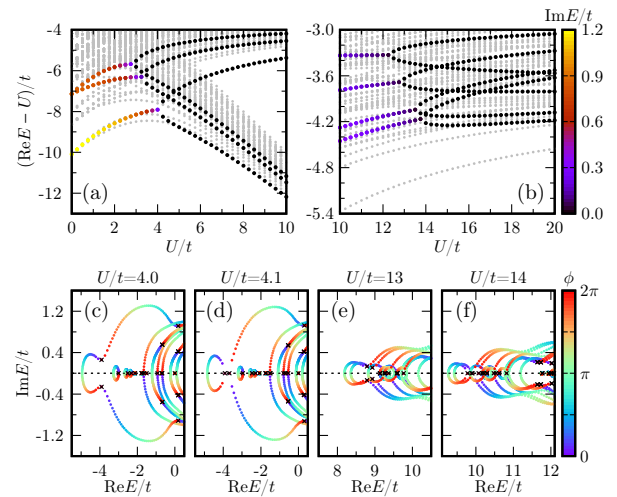


FIG. 4. Real components of eigenvalues varying with Coulomb repulsion U for (a) $0 \leq U/t \leq 10$ and (b) $10 \leq U/t \leq 20$. (a) and (b) represent the eigenvalue spectrum for no and one doubton-holon sector, respectively. We highlight a few eigenpairs, which perform the transition from complex conjugate pair to two pure real numbers, using color map. (c)–(f) show the spectral evolutions of eigenvalues of $k = 0$ and $S_z = 0$ eigenstates as a function of the gauge flux ϕ under TBC. All results are obtained when $A = 0.3$ and $L = 8$.

the Hermitian nature of the Coulomb interaction part in Eq. 13, all eigenvalues asymptotically converge to real numbers in the U -infinite limit even for PBC. All complex conjugate eigenpairs in finite U eventually transform into two real eigenvalues. This transition involves the gradual separation of two real eigenvalues, following the merging of complex conjugate eigenpairs along the real axis. This spectral behavior resembles the \mathcal{PT} -phase transition [64, 65]. Figure 4(a) and (b) well depict the sequential occurrences of these transitions when U gradually increases.

We further examine the evolution of complex eigenvalues in the presence of the gauge flux ϕ under TBC. As shown in Fig. 4(c)–(f), complex conjugate eigenpair are connected by the ϕ evolution before the transition, while that eigenpair get separated after the transition. It implies the winding number in Eq. 5 changes undergoing the transition, giving the different point-gap topology [56, 64]. Moreover, two eigenstates of the eigenpair involved in the transition collapse into a singular state at the transition point (see SM [59]). The transition point of the winding number is identified as \mathcal{PT} -like topological transitions accompanying the exceptional point. (see SM [59] for the topological transitions as a function of A).

Summary and discussion– We investigate the intriguing behavior of the many-body NHSE and unique features of eigenspectra in the half-filled interaction Hatano-Nelson model of spin-half fermions. We discover that strong interactions suppress doubton-holon

excitations in the ground state, leading to the absence of the NHSE. However, excited eigenstates still exhibit these excitations, driven by non-reciprocal hopping, which causes doublons and holons to move in opposite directions. The spatial segregation of doublon-holon pairs serves the hallmark of the many-body skin modes. Moreover, these modes are attributed to the bulk-boundary correspondence mediated by the point gap topology within complex many-body eigenspectrums.

Experimentally, realizing these effects can be challenging, but open quantum systems such as ultracold atoms can be a promising platform. Experiments with bosonic ultracold atoms have already shown skin effects [13]. Because the dynamics of the systems is governed by the Liouvillian master equations, exploring the interplay between many-body effects and Liouvillian skin effects [15, 41, 66, 67] in such systems holds great potential for unveiling novel physical phenomena of non-Hermitian many-body physics.

Acknowledgements— We acknowledge Jung-Wan Ryu, Hee Chul Park, and Sonu Verma for fruitful discussion. This work was supported from the Institute for Basic Science in the Republic of Korea through the Project No. IBS-R024-D1. This work was supported by the National Research Foundation of Korea (NRF) grant funded by the Korea government (MSIT) (Grants No. RS-2023-00252085 and No. RS-2023-00218998).

-
- [1] C. M. Bender, Making sense of non-Hermitian Hamiltonians, *Rep. on Prog. Phys.* **70**, 947 (2007).
- [2] K. Jones-Smith and H. Mathur, Non-Hermitian quantum Hamiltonians with PT symmetry, *Phys. Rev. A* **82**, 042101 (2010).
- [3] C. M. Bender, I. Cervero-Pelaez, K. A. Milton, and K. Shajesh, PT -symmetric quantum electrodynamics, *Phys. Lett. B* **613**, 97 (2005).
- [4] Alexandre, C. M. Jean Bender, and P. Millington, Non-Hermitian extension of gauge theories and implications for neutrino physics, *J. High Energ. Phys.* **2015**, 111.
- [5] L. Feng, R. El-Ganainy, and L. Ge, Non-Hermitian photonics based on parity-time symmetry, *Nat. Photonics* **11**, 752 (2017).
- [6] Ş. K. Özdemir, S. Rotter, F. Nori, and L. Yang, Parity-time symmetry and exceptional points in photonics, *Nat. Mater.* **18**, 783 (2019).
- [7] M.-A. M. Miri and A. Alù, Exceptional points in optics and photonics, *Science* **363**, eaar7709 (2019).
- [8] T. Ozawa, H. M. Price, A. Amo, N. Goldman, M. Hafezi, L. Lu, M. C. Rechtsman, D. Schuster, J. Simon, O. Zilberberg, and I. Carusotto, Topological photonics, *Rev. Mod. Phys.* **91**, 015006 (2019).
- [9] S. Longhi, Stochastic non-Hermitian skin effect, *Opt. Lett.* **45**, 5250 (2020).
- [10] X. Zhu, H. Wang, S. K. Gupta, H. Zhang, B. Xie, M. Lu, and Y. Chen, Photonic non-Hermitian skin effect and non-Bloch bulk-boundary correspondence, *Phys. Rev. Res.* **2**, 013280 (2020).
- [11] Y. Takasu, T. Yagami, Y. Ashida, R. Hamazaki, Y. Kuno, and Y. Takahashi, PT -symmetric non-Hermitian quantum many-body system using ultracold atoms in an optical lattice with controlled dissipation, *Prog. Theor. Exp. Phys.* **2020**, 12A110 (2020).
- [12] S. Guo, C. Dong, F. Zhang, J. Hu, and Z. Yang, Theoretical prediction of a non-Hermitian skin effect in ultracold-atom systems, *Phys. Rev. A* **106**, L061302 (2022).
- [13] Q. Liang, D. Xie, Z. Dong, H. Li, H. Li, B. Gadway, W. Yi, and B. Yan, Dynamic Signatures of Non-Hermitian Skin Effect and Topology in Ultracold Atoms, *Phys. Rev. Lett.* **129**, 070401 (2022).
- [14] L. Zhou, H. Li, W. Yi, and X. Cui, Engineering non-Hermitian skin effect with band topology in ultracold gases, *Commun. Phys.* **5**, 252 (2022).
- [15] S. Hamanaka, K. Yamamoto, and T. Yoshida, Interaction-induced Liouvillian skin effect in a fermionic chain with two-body loss, (2023), [arXiv:2305.19697](https://arxiv.org/abs/2305.19697).
- [16] N. Hatano and D. R. Nelson, Localization Transitions in Non-Hermitian Quantum Mechanics, *Phys. Rev. Lett.* **77**, 570 (1996).
- [17] N. Hatano and D. R. Nelson, Non-Hermitian delocalization and eigenfunctions, *Phys. Rev. B* **58**, 8384 (1998).
- [18] T. Fukui and N. Kawakami, Breakdown of the Mott insulator: Exact solution of an asymmetric Hubbard model, *Phys. Rev. B* **58**, 16051 (1998).
- [19] V. Kozii and L. Fu, Non-Hermitian Topological Theory of Finite-Lifetime Quasiparticles: Prediction of Bulk Fermi Arc Due to Exceptional Point, (2017), [arXiv:1708.05841](https://arxiv.org/abs/1708.05841).
- [20] T. Yoshida, R. Peters, and N. Kawakami, Non-Hermitian perspective of the band structure in heavy-fermion systems, *Phys. Rev. B* **98**, 035141 (2018).
- [21] Y. Nagai, Y. Qi, H. Isobe, V. Kozii, and L. Fu, DMFT Reveals the Non-Hermitian Topology and Fermi Arcs in Heavy-Fermion Systems, *Phys. Rev. Lett.* **125**, 227204 (2020).
- [22] R. Rausch, R. Peters, and T. Yoshida, Exceptional points in the one-dimensional Hubbard model, *New J. Phys.* **23**, 013011 (2021).
- [23] Z. Ren, D. Liu, E. Zhao, C. He, K. K. Pak, J. Li, and G.-B. Jo, Chiral control of quantum states in non-Hermitian spin-orbit-coupled fermions, *Nature Physics* **18**, 385 (2022).
- [24] Z. Gong, Y. Ashida, K. Kawabata, K. Takasan, S. Higashikawa, and M. Ueda, Topological Phases of Non-Hermitian Systems, *Phys. Rev. X* **8**, 031079 (2018).
- [25] S. Yao and Z. Wang, Edge States and Topological Invariants of Non-Hermitian Systems, *Phys. Rev. Lett.* **121**, 086803 (2018).
- [26] S. Yao, F. Song, and Z. Wang, Non-Hermitian Chern Bands, *Phys. Rev. Lett.* **121**, 136802 (2018).
- [27] K. Kawabata, K. Shiozaki, M. Ueda, and M. Sato, Symmetry and Topology in Non-Hermitian Physics, *Phys. Rev. X* **9**, 041015 (2019).
- [28] F. Song, S. Yao, and Z. Wang, Non-Hermitian Topological Invariants in Real Space, *Phys. Rev. Lett.* **123**, 246801 (2019).
- [29] K. Yokomizo and S. Murakami, Non-Bloch Band Theory of Non-Hermitian Systems, *Phys. Rev. Lett.* **123**, 066404 (2019).
- [30] T.-S. Deng and W. Yi, Non-Bloch topological

- invariants in a non-Hermitian domain wall system, *Phys. Rev. B* **100**, 035102 (2019).
- [31] N. Okuma, K. Kawabata, K. Shiozaki, and M. Sato, Topological Origin of Non-Hermitian Skin Effects, *Phys. Rev. Lett.* **124**, 086801 (2020).
- [32] D. S. Borgnia, A. J. Kruchkov, and R.-J. Slager, Non-Hermitian Boundary Modes and Topology, *Phys. Rev. Lett.* **124**, 056802 (2020).
- [33] E. J. Bergholtz, J. C. Budich, and F. K. Kunst, Exceptional topology of non-Hermitian systems, *Rev. Mod. Phys.* **93**, 015005 (2021).
- [34] K. Ding, C. Fang, and G. Ma, Non-Hermitian topology and exceptional-point geometries, *Nat. Rev. Phys.* **4**, 745 (2022).
- [35] R. Lin, T. Tai, L. Li, and C. H. Lee, Topological non-Hermitian skin effect, *Front. Phys.* **18**, 53605 (2023).
- [36] K. Kawabata, T. Numasawa, and S. Ryu, Entanglement Phase Transition Induced by the Non-Hermitian Skin Effect, *Phys. Rev. X* **13**, 021007 (2023).
- [37] C. H. Lee and R. Thomale, Anatomy of skin modes and topology in non-Hermitian systems, *Phys. Rev. B* **99**, 201103 (2019).
- [38] H. Jiang, L.-J. Lang, C. Yang, S.-L. Zhu, and S. Chen, Interplay of non-Hermitian skin effects and Anderson localization in nonreciprocal quasiperiodic lattices, *Phys. Rev. B* **100**, 054301 (2019).
- [39] K.-I. Imura and Y. Takane, Generalized bulk-edge correspondence for non-Hermitian topological systems, *Phys. Rev. B* **100**, 165430 (2019).
- [40] K. Zhang, Z. Yang, and C. Fang, Correspondence between Winding Numbers and Skin Modes in Non-Hermitian Systems, *Phys. Rev. Lett.* **125**, 126402 (2020).
- [41] Z. Yang, K. Zhang, C. Fang, and J. Hu, Non-Hermitian Bulk-Boundary Correspondence and Auxiliary Generalized Brillouin Zone Theory, *Phys. Rev. Lett.* **125**, 226402 (2020).
- [42] Y. Yi and Z. Yang, Non-Hermitian Skin Modes Induced by On-Site Dissipations and Chiral Tunneling Effect, *Phys. Rev. Lett.* **125**, 186802 (2020).
- [43] H. Schomerus, Nonreciprocal response theory of non-Hermitian mechanical metamaterials: Response phase transition from the skin effect of zero modes, *Phys. Rev. Res.* **2**, 013058 (2020).
- [44] H. Ghaemi-Dizicheh and H. Schomerus, Compatibility of transport effects in non-Hermitian nonreciprocal systems, *Phys. Rev. A* **104**, 023515 (2021).
- [45] A. Ghatak, M. Brandenbourger, J. van Wezel, and C. Coulais, Observation of non-Hermitian topology and its bulk-edge correspondence in an active mechanical metamaterial, *Proc. Natl. Acad. Sci.* **117**, 29561 (2020).
- [46] T. Helbig, T. Hofmann, S. Imhof, M. Abdelghany, T. Kiessling, L. W. Molenkamp, C. H. Lee, A. Szameit, M. Greiter, and R. Thomale, Generalized bulk-boundary correspondence in non-Hermitian topoelectrical circuits, *Nat. Phys.* **16**, 747 (2020).
- [47] S. Weidemann, M. Kremer, T. Helbig, T. Hofmann, A. Stegmaier, M. Greiter, R. Thomale, and A. Szameit, Topological funneling of light, *Science* **368**, 311 (2020).
- [48] J. Claes and T. L. Hughes, Skin effect and winding number in disordered non-Hermitian systems, *Phys. Rev. B* **103**, L140201 (2021).
- [49] S. Longhi, Spectral deformations in non-Hermitian lattices with disorder and skin effect: A solvable model, *Phys. Rev. B* **103**, 144202 (2021).
- [50] K.-M. Kim and M. J. Park, Disorder-driven phase transition in the second-order non-Hermitian skin effect, *Phys. Rev. B* **104**, L121101 (2021).
- [51] Z. Gu, H. Gao, H. Xue, J. Li, Z. Su, and J. Zhu, Transient non-Hermitian skin effect, *Nat. Commun.* **13**, 7668 (2022).
- [52] W. Wang, X. Wang, and G. Ma, Non-Hermitian morphing of topological modes, *Nature* **608**, 50 (2022).
- [53] E. Lee, H. Lee, and B.-J. Yang, Many-body approach to non-Hermitian physics in fermionic systems, *Phys. Rev. B* **101**, 121109 (2020).
- [54] S.-B. Zhang, M. M. Denner, T. Bzdušek, M. A. Sentef, and T. Neupert, Symmetry breaking and spectral structure of the interacting Hatano-Nelson model, *Phys. Rev. B* **106**, L121102 (2022).
- [55] K. Kawabata, K. Shiozaki, and S. Ryu, Many-body topology of non-Hermitian systems, *Phys. Rev. B* **105**, 165137 (2022).
- [56] F. Alsallom, L. Herviou, O. V. Yazyev, and M. Brzezińska, Fate of the non-Hermitian skin effect in many-body fermionic systems, *Phys. Rev. Res.* **4**, 033122 (2022).
- [57] T. Liu, J. J. He, T. Yoshida, Z.-L. Xiang, and F. Nori, Non-Hermitian topological Mott insulators in one-dimensional fermionic superlattices, *Phys. Rev. B* **102**, 235151 (2020).
- [58] S. Longhi, Spectral structure and doublon dissociation in the two-particle non-Hermitian Hubbard model, (2023), [arXiv:2308.04505](https://arxiv.org/abs/2308.04505).
- [59] See Supplemental Material for the detail on the Hamiltonian properties, the Non-Hermitian skin effect, the effective Hamiltonian in strong coupling limit, eigenspectrum at $U = 0$, the orthonormality property at the topological transitions, and the topological transition under an imaginary gauge flux.
- [60] A. Mostafazadeh, Pseudo-Hermiticity versus PT-symmetry. II. A complete characterization of non-Hermitian Hamiltonians with a real spectrum, *J. Math. Phys.* **43**, 2814 (2002).
- [61] A. Mostafazadeh, Pseudo-Hermiticity versus PT symmetry: The necessary condition for the reality of the spectrum of a non-Hermitian Hamiltonian, *J. Math. Phys.* **43**, 205 (2002).
- [62] S. Heußen, C. D. White, and G. Refael, Extracting many-body localization lengths with an imaginary vector potential, *Phys. Rev. B* **103**, 064201 (2021).
- [63] F. H. L. Essler, H. Frahm, F. Göhmann, A. Klümper, and V. E. Korepin, *The one-dimensional Hubbard model* (Cambridge University Press, Cambridge, 2010).
- [64] S. Longhi, Topological Phase Transition in non-Hermitian Quasicrystals, *Phys. Rev. Lett.* **122**, 237601 (2019).
- [65] S. Longhi, Probing non-Hermitian skin effect and non-Bloch phase transitions, *Phys. Rev. Res.* **1**, 023013 (2019).
- [66] T. Haga, M. Nakagawa, R. Hamazaki, and M. Ueda, Liouvillian Skin Effect: Slowing Down of Relaxation Processes without Gap Closing, *Phys. Rev. Lett.* **127**, 070402 (2021).
- [67] H. Li, H. Wu, W. Zheng, and W. Yi, Many-body non-Hermitian skin effect under dynamic gauge coupling, *Phys. Rev. Res.* **5**, 033173 (2023).

Supplemental Material: Point-gap topology and skin effect of the doublon-holon excitations in non-reciprocal many-body systems

HAMILTONIAN PROPERTIES

Hamiltonian

We consider the one-dimensional Hatano-Nelson model of spin-half fermions described by the following Hamiltonian:

$$H = -t \sum_{l=0}^{L-2} \sum_{\sigma} \left(e^A c_{l+1,\sigma}^{\dagger} c_{l,\sigma} + e^{-A} c_{l,\sigma}^{\dagger} c_{l+1,\sigma} \right) + U \sum_{l=0}^{L-1} n_{l,\uparrow} n_{l,\downarrow} + H_B \quad (1)$$

where $c_{l,\sigma}^{\dagger}$ ($c_{l,\sigma}$) represents the creation (annihilation) operator of a fermion with spin σ ($=\uparrow, \downarrow$) at the l th site, and $n_{l,\sigma} = c_{l,\sigma}^{\dagger} c_{l,\sigma}$ is the number operator at the site. The lattice size is denoted by L and A refers to the imaginary vector potential to give rise to the non-reciprocal hopping [16, 17]. Additionally, H_B accounts for the hopping Hamiltonian between fermions at the boundary and can be adopted differently for periodic, open, and twisted boundary conditions as follows: H_B can be given as

$$H_B^{PBC} = -t \sum_{\sigma} \left(e^A c_{0,\sigma}^{\dagger} c_{L-1,\sigma} + e^{-A} c_{L-1,\sigma}^{\dagger} c_{0,\sigma} \right), \quad (2a)$$

$$H_B^{OBC} = 0, \quad (2b)$$

$$H_B^{TBC} = -t \sum_{\sigma} \left(e^{A+i\phi} c_{0,\sigma}^{\dagger} c_{L-1,\sigma} + e^{-A-i\phi} c_{L-1,\sigma}^{\dagger} c_{0,\sigma} \right), \quad (2c)$$

where ϕ denotes the $U(1)$ -gauge (magnetic) flux. For twisted boundary condition, we can perform a unitary transformation of local fermionic operators as follows:

$$c_{l\sigma}^{\dagger} \rightarrow \tilde{c}_{l\sigma}^{\dagger} = e^{il\phi/L} c_{l\sigma}^{\dagger}, \quad c_{l\sigma} \rightarrow \tilde{c}_{l\sigma} = e^{-il\phi/L} c_{l\sigma}. \quad (3)$$

This transformation allows us to obtain an effective periodic Hamiltonian as follows:

$$H = -t \sum_{l=0}^{L-2} \sum_{\sigma} \left(e^{A+i\phi/L} \tilde{c}_{l+1,\sigma}^{\dagger} \tilde{c}_{l,\sigma} + e^{-A-i\phi/L} \tilde{c}_{l,\sigma}^{\dagger} \tilde{c}_{l+1,\sigma} \right) + U \sum_{l=0}^{L-1} \tilde{n}_{l,\uparrow} \tilde{n}_{l,\downarrow} + \tilde{H}_B, \quad (4)$$

where $\tilde{n}_{l,\sigma} = \tilde{c}_{l,\sigma}^{\dagger} \tilde{c}_{l,\sigma}$ and $\tilde{H}_B = -t \sum_{\sigma} \left(e^{A+i\phi/L} \tilde{c}_{0,\sigma}^{\dagger} \tilde{c}_{L-1,\sigma} + e^{-A-i\phi/L} \tilde{c}_{L-1,\sigma}^{\dagger} \tilde{c}_{0,\sigma} \right)$.

Pseudo-Hermiticity

Similar to the spinless Hatano-Nelson model [54], the Hamiltonian of Eq. 1 can exhibit the pseudo-Hermiticity for the twisted (periodic) boundary condition with respect to the \mathcal{PT} symmetry. Let \mathcal{P} and \mathcal{T} be inversion and time-reversal operators, respectively. We can get the following relations:

$$(\mathcal{PT}) c_{l,\sigma}^{\dagger} (\mathcal{PT})^{-1} = (-1)^{n_{\sigma}} c_{L-1-l,\sigma}^{\dagger}, \quad (\mathcal{PT}) e^{i\phi} (\mathcal{PT})^{-1} = e^{-i\phi}, \quad (5)$$

where $n_\sigma = 0$ (1) for $\sigma = \uparrow$ (\downarrow) and $\bar{\sigma}$ represents an opposite spin of σ . By applying the \mathcal{PT} operator on the Hamiltonian H , we expand the equation as follows:

$$\begin{aligned}
(\mathcal{PT}) H (\mathcal{PT})^{-1} &= -t \sum_{l=0}^{L-2} \sum_{\sigma} (\mathcal{PT}) \left(e^A c_{l+1,\sigma}^\dagger c_{l,\sigma} + e^{-A} c_{l,\sigma}^\dagger c_{l+1,\sigma} \right) (\mathcal{PT})^{-1} + U \sum_{l=0}^{L-1} (\mathcal{PT}) n_{l,\uparrow} n_{l,\downarrow} (\mathcal{PT})^{-1} \\
&\quad - t \sum_{\sigma} (\mathcal{PT}) \left(e^{A+i\phi} c_{0,\sigma}^\dagger c_{L-1,\sigma} + e^{-A-i\phi} c_{L-1,\sigma}^\dagger c_{0,\sigma} \right) (\mathcal{PT})^{-1} \\
&= -t \sum_{l=0}^{L-2} \sum_{\sigma} \left(e^A c_{L-2-l,\bar{\sigma}}^\dagger c_{L-1-l,\bar{\sigma}} + e^{-A} c_{L-1-l,\bar{\sigma}}^\dagger c_{L-2-l,\bar{\sigma}} \right) + U \sum_{l=0}^{L-1} n_{L-1-l,\downarrow} n_{L-1-l,\uparrow} \\
&\quad - t \sum_{\sigma} \left(e^{A-i\phi} c_{0,\bar{\sigma}}^\dagger c_{L-1,\bar{\sigma}} + e^{-A+i\phi} c_{0,\bar{\sigma}}^\dagger c_{L-1,\bar{\sigma}} \right). \tag{6}
\end{aligned}$$

By replacing the site index ($l' = L - 2 - l$ and $l'' = L - 1 - l$) and spin state ($\sigma' = \bar{\sigma}$), we get the equation as follows:

$$\begin{aligned}
(\mathcal{PT}) H (\mathcal{PT})^{-1} &= -t \sum_{l'=0}^{L-2} \sum_{\sigma'} \left(e^A c_{l'+1,\sigma'}^\dagger c_{l',\sigma'} + e^{-A} c_{l',\sigma'}^\dagger c_{l'+1,\sigma'} \right) + U \sum_{l''=0}^{L-1} n_{l'',\uparrow} n_{l'',\downarrow} \\
&\quad - t \sum_{\sigma'} \left(e^{A-i\phi} c_{L-1,\sigma'}^\dagger c_{0,\sigma'} + e^{-A+i\phi} c_{0,\sigma'}^\dagger c_{L-1,\sigma'} \right) \\
&= H^\dagger. \tag{7}
\end{aligned}$$

Thus, H is the psuedo-Hermitian operator with respect to the \mathcal{PT} symmetric operator. Consequently, the eigenvalues for the twisted (periodic) boundary condition should either be real or come in complex-conjugate pairs [61].

Symmetry

Let \hat{N} and \hat{S}_z be operators for the total number of fermions and the z -component of the total spin, given as $\hat{N} = \sum_{l=0}^{L-1} (n_{l,\uparrow} + n_{l,\downarrow})$ and $\hat{S}_z = \sum_{l=0}^{L-1} (n_{l,\uparrow} - n_{l,\downarrow})$. Importantly, the Hamiltonian H commutes both \hat{N} and \hat{S}_z operators, regardless of the selected A value and boundary condition. This implies that we can determine the eigenvalues of the Hamiltonian by considering the subspace in which both \hat{N} and \hat{S}_z are constant. For N -fermion systems, we can conveniently adopt basis states for the Hilbert space as follows:

$$|\Psi_n\rangle = \prod_{j=1}^N c_{l_{nj},\sigma_{nj}}^\dagger |vac\rangle, \tag{8}$$

where l_{nj} and σ_{nj} denote the site index and spin state of the j th fermion for the n th state, respectively, and $|vac\rangle$ represents the vacuum state.

In periodic and twisted boundary conditions, the Hamiltonian exhibits the translation symmetry. We can take into account L number of translation operators, defined as $T_l c_{l',\sigma}^\dagger T_l^{-1} = c_{l'+l \bmod L,\sigma}^\dagger$ ($0 \leq l, l' < L$). T_0 corresponds to the identity operator. With the translation symmetry, the many-body states can be characterized with the crystal momentum $k \in \{0, 2\pi/L, \dots, 2\pi(L-1)/L\}$. The translation-symmetrized basis states can be expressed as follows:

$$|\Psi_n(k)\rangle = \frac{1}{\sqrt{N_{nk}}} \sum_{l=0}^{L-1} e^{-ikl} T_l |\Psi_n\rangle, \tag{9}$$

where N_{nk} is the normalization factor and $|\Psi_n\rangle$ is the representative state for the n th basis state. $T_l |\Psi_n\rangle$ can be obtained as follows:

$$T_l |\Psi_n\rangle = \prod_{j=1}^N T_l c_{l_{nj},\sigma_{nj}}^\dagger T_l^{-1} |vac\rangle = \prod_{j=1}^N c_{l_{nj}+l \bmod L,\sigma_{nj}}^\dagger |vac\rangle. \tag{10}$$

By utilizing the translation symmetry and expressing the basis states in terms of crystal momentum, we can effectively reduce the Hilbert space, making it more tractable to calculate the eigenvalues and eigenstates of the Hamiltonian.

Non-interacting case ($U=0$)

Let H_t be the Hamiltonian for $U = 0$ which is given as

$$H_t = -t \sum_{l=0}^{L-2} \sum_{\sigma} \left(e^A c_{l+1,\sigma}^{\dagger} c_{l,\sigma} + e^{-A} c_{l,\sigma}^{\dagger} c_{l+1,\sigma} \right) + H_B. \quad (11)$$

To verify the normality of non-Hermitian H_t , we calculate the commutator $[H_t, H_t^{\dagger}]$ as following:

$$\begin{aligned} [H_t, H_t^{\dagger}] &= t^2 \sum_{l=1}^{L-2} \sum_{\sigma} \left\{ e^{2A} \left(c_{l+1,\sigma}^{\dagger} c_{l+1,\sigma} - c_{l,\sigma}^{\dagger} c_{l,\sigma} \right) + e^{-2A} \left(c_{l,\sigma}^{\dagger} c_{l,\sigma} - c_{l+1,\sigma}^{\dagger} c_{l+1,\sigma} \right) \right\} \\ &\quad + st^2 \sum_{\sigma} \left\{ e^{2A} \left(c_{0,\sigma}^{\dagger} c_{0,\sigma} - c_{L-1,\sigma}^{\dagger} c_{L-1,\sigma} \right) + e^{-2A} \left(c_{L-1,\sigma}^{\dagger} c_{L-1,\sigma} - c_{0,\sigma}^{\dagger} c_{0,\sigma} \right) \right\} \\ &= 2t^2 \sinh(2A) (1-s) \sum_{\sigma} \left(c_{L-1,\sigma}^{\dagger} c_{L-1,\sigma} - c_{0,\sigma}^{\dagger} c_{0,\sigma} \right), \end{aligned} \quad (12)$$

where $s = 1$ ($s = 0$) for the periodic (open) boundary condition. Notably, when $[H_t, H_t^{\dagger}] = 0$ is satisfied, H_t becomes a normal operator, enabling us to construct orthonormal right and left eigenstates, even if the eigenvalues may be complex. Consequently, all eigenstates for the periodic boundary are orthonormal each other when $U = 0$. However, for the open boundary condition, $[H_t, H_t^{\dagger}]$ is no longer zero when $A \neq 0$. In this case, the orthonormality of right and left eigenstates is not mandatory.

Open boundary condition

In open boundary condition, the one-dimensional Hatano-Nelson model of spin-half fermions is given as

$$H = -t \sum_{l=0}^{L-2} \sum_{\sigma} \left(e^A c_{l+1,\sigma}^{\dagger} c_{l,\sigma} + e^{-A} c_{l,\sigma}^{\dagger} c_{l+1,\sigma} \right) + U \sum_{l=0}^{L-1} c_{l,\uparrow}^{\dagger} c_{l,\uparrow} c_{l,\downarrow}^{\dagger} c_{l,\downarrow}. \quad (13)$$

For the non-orthonormality property of eigenstates, we introduce new local fermionic operators $g_{l,\sigma}^{\dagger}$ and $\bar{g}_{l,\sigma}$, defined as $g_{l,\sigma}^{\dagger} = e^{lA} c_{l,\sigma}^{\dagger}$ and $\bar{g}_{l,\sigma} = e^{-lA} c_{l,\sigma}$. The Hamiltonian of Eq. 13 is rewritten with the pseudo-Hermitian form as following:

$$H = -t \sum_{l=0}^{L-2} \sum_{\sigma} \left(g_{l+1,\sigma}^{\dagger} \bar{g}_{l,\sigma} + g_{l,\sigma}^{\dagger} \bar{g}_{l+1,\sigma} \right) + U \sum_{l=0}^{L-1} g_{l,\uparrow}^{\dagger} \bar{g}_{l,\uparrow} g_{l,\downarrow}^{\dagger} \bar{g}_{l,\downarrow}. \quad (14)$$

In contrast, in periodic (twisted) boundary conditions, the boundary Hamiltonian H_B is written as following:

$$H_B = -t \sum_{\sigma} \left(e^{LA} g_{0,\sigma}^{\dagger} \bar{g}_{L-1,\sigma} + e^{-LA} g_{L-1,\sigma}^{\dagger} \bar{g}_{0,\sigma} \right). \quad (15)$$

Because of uncompensated phase terms $e^{\pm LA}$, H_B cannot be expressed with the pseudo-Hermitian form like Eq. 14.

When the imaginary vector potential A is set to be zero ($A = 0$), the Hamiltonian of Eq. 13 becomes Hermitian, resulting in real eigenvalues and orthonormal eigenstates. The eigenstates of the Hamiltonian $H_{A=0}$ (Hamiltonian with $A = 0$) are given as $H_{A=0} |\Psi_E^0\rangle = E |\Psi_E^0\rangle$, and it can be expressed with the linear combination of orthonormal basis states: $|\Psi_E^0\rangle = \sum_n C_n^E |\Psi_n\rangle$, where E is the eigenvalue and $|\Psi_n\rangle$ is defined in Eq. 8. The coefficients C_n^E can be determined by solving the following eigenproblem:

$$\sum_m h_{nm}^0 C_m^E = E C_n^E, \quad (16)$$

where $h_{nm}^0 = \langle \Psi_n | H_{A=0} | \Psi_m \rangle$. Because $H_{A=0}$ is the real-value operator, we can get $h_{nm}^0 = h_{mn}^0$.

In the case when $A \neq 0$, the Hamiltonian is no longer Hermitian due to non-zero non-reciprocal hopping, possibly leading to complex eigenvalues and non-orthonormal right and left eigenstates. We introduce non-orthonormal basis states defined as follows:

$$|\Psi_n^R\rangle = \prod_{j=1}^N g_{l_{nj}, \sigma_{nj}}^\dagger |vac\rangle = e^{A \sum_{j=1}^N l_{nj}} |\Psi_n\rangle, \quad (17a)$$

$$|\Psi_n^L\rangle = \prod_{j=1}^N \bar{g}_{l_{nj}, \sigma_{nj}}^\dagger |vac\rangle = e^{-A \sum_{j=1}^N l_{nj}} |\Psi_n\rangle, \quad (17b)$$

to express non-orthonormal right and left eigenstates of Eq. 13, respectively. Considering Eq. 8 and 17, we can deduce that $\langle \Psi_n^L | g_{l, \sigma}^\dagger \bar{g}_{l', \sigma'} | \Psi_m^R \rangle = e^{A(l-l')} e^{A \sum_{j=1}^N (l_{mj} - l_{nj})} \langle \Psi_n | c_{l, \sigma}^\dagger c_{l', \sigma'} | \Psi_m \rangle$. Here, the term $\langle \Psi_n | c_{l, \sigma}^\dagger c_{l', \sigma'} | \Psi_m \rangle$ has a non-zero value only when $l \in \{l_{n1}, \dots, l_{nN}\}$, $l' \in \{l_{m1}, \dots, l_{mN}\}$, and $\{l_{n1}, \dots, l_{nN}\} - \{l\} = \{l_{m1}, \dots, l_{mN}\} - \{l'\}$. We can get $\langle \Psi_n | c_{l, \sigma}^\dagger c_{l', \sigma'} | \Psi_m \rangle = \langle \Psi_n^L | g_{l, \sigma}^\dagger \bar{g}_{l', \sigma'} | \Psi_m^R \rangle$. As a result, we can easily derive following relation:

$$\langle \Psi_n | H_{A=0} | \Psi_m \rangle = \langle \Psi_m | H_{A=0} | \Psi_n \rangle = \langle \Psi_n^L | H | \Psi_m^R \rangle = \langle \Psi_m^R | H^\dagger | \Psi_n^L \rangle = \langle \Psi_n^R | H^\dagger | \Psi_m^L \rangle, \quad (18)$$

because $H_{A=0}$ is Hermitian.

Let E_R (E_L) and $|\Psi_{E_R}^R\rangle$ ($|\Psi_{E_L}^L\rangle$) be the right (left) eigenvalue and eigenstate of Eq. 13, respectively. Utilizing the eigenvalue equations $H |\Psi_{E_R}^R\rangle = E_R |\Psi_{E_R}^R\rangle$ ($H^\dagger |\Psi_{E_L}^L\rangle = E_L^* |\Psi_{E_L}^L\rangle$), along with the biorthonormal property $\sum_n |\Psi_n^R\rangle \langle \Psi_n^L| = \sum_n |\Psi_n\rangle \langle \Psi_n| = \mathbf{I}$ ($\sum_n |\Psi_n^L\rangle \langle \Psi_n^R| = \sum_n |\Psi_n\rangle \langle \Psi_n| = \mathbf{I}$), we obtain the following equations:

$$\sum_m \langle \Psi_n^L | H | \Psi_m^R \rangle \langle \Psi_m^L | \Psi_{E_R}^R \rangle = E_R \langle \Psi_n^L | \Psi_{E_R}^R \rangle, \quad (19a)$$

$$\sum_m \langle \Psi_n^R | H^\dagger | \Psi_m^L \rangle \langle \Psi_m^R | \Psi_{E_L}^L \rangle = E_L^* \langle \Psi_n^R | \Psi_{E_L}^L \rangle. \quad (19b)$$

Since Eq. 18 and 19, we deduce the following eigenproblems:

$$\sum_m h_{nm}^0 \langle \Psi_m^L | \Psi_{E_R}^R \rangle = E_R \langle \Psi_n^L | \Psi_{E_R}^R \rangle, \quad (20a)$$

$$\sum_m h_{nm}^0 \langle \Psi_m^R | \Psi_{E_L}^L \rangle = E_L^* \langle \Psi_n^R | \Psi_{E_L}^L \rangle. \quad (20b)$$

Equation 16 supports the solution with $E_R = E_L^* = E$ and $\langle \Psi_n^L | \Psi_{E_R}^R \rangle = \langle \Psi_n^R | \Psi_{E_L}^L \rangle = C_n^E$. The left and right eigenvalues of Eq. 13 in open boundary condition are purely real and remain robust regardless of the strength of A . Right and left eigenstates are given as following:

$$|\Psi_E^R\rangle = \sum_n C_n^E |\Psi_n^R\rangle = \sum_n e^{A \sum_j l_{nj}} C_n^E |\Psi_n\rangle, \quad (21a)$$

$$|\Psi_E^L\rangle = \sum_n C_n^E |\Psi_n^L\rangle = \sum_n e^{-A \sum_j l_{nj}} C_n^E |\Psi_n\rangle. \quad (21b)$$

In contrast with the Hermitian case ($A = 0$), eigenstates are not orthonormal each other when $A \neq 0$ due to the factor $e^{A \sum_j l_{nj}}$ ($e^{-A \sum_j l_{nj}}$) of basis state $|\Psi_n^R\rangle$ ($|\Psi_n^L\rangle$).

The complete set of real eigenvalues of non-Hermitian Hamiltonians is directly linked to the concept of pseudo-Hermiticity of Hamiltonian [60]. To explore this, we introduce an invertible linear operator S defined as:

$$S = \sum_n |\Psi_n^R\rangle \langle \Psi_n|, \quad (22)$$

where $|\Psi_n\rangle$ and $|\Psi_n^R\rangle$ are the n th orthonormal basis states and non-orthonormal basis states for right eigenstates of H , respectively. Utilizing the biorthonormal property, we can verify that the inverse operator of S is given as:

$$S^{-1} = \sum_n |\Psi_n\rangle \langle \Psi_n^L|, \quad (23)$$

where $|\Psi_n^L\rangle$ is the n th non-orthonormal basis states for left eigenstate of H . Utilizing Eqs. 18, 22 and 23, we can deduce the following relation:

$$\langle \Psi_n | S^{-1} H S | \Psi_m \rangle = \sum_{n'm'} \langle \Psi_n | \Psi_{n'} \rangle \langle \Psi_{n'}^L | H | \Psi_{m'}^R \rangle \langle \Psi_{m'} | \Psi_n \rangle = \langle \Psi_n^L | H | \Psi_m^R \rangle = \langle \Psi_n | H_{A=0} | \Psi_m \rangle. \quad (24)$$

We arrive at the following relation:

$$H_{A=0} = S^{-1} H S, \quad (25)$$

where $H_{A=0}$ is the Hermitian operator. Moreover, we obtain $SS^\dagger = \sum_n |\Psi_n^R\rangle \langle \Psi_n^R|$ and $(SS^\dagger)^{-1} = \sum_n |\Psi_n^L\rangle \langle \Psi_n^L|$. We can deduce the following relation:

$$\langle \Psi_n^R | (SS^\dagger)^{-1} H S S^\dagger | \Psi_m^L \rangle = \sum_{n'm'} \langle \Psi_n^R | \Psi_{n'}^L \rangle \langle \Psi_{n'}^L | H | \Psi_{m'}^R \rangle \langle \Psi_{m'}^R | \Psi_m^L \rangle = \langle \Psi_n^L | H | \Psi_m^R \rangle = \langle \Psi_n^R | H^\dagger | \Psi_m^L \rangle, \quad (26)$$

where we utilize Eq. 18. We can prove that H is the SS^\dagger -pseudo-Hermitian such that $H = (SS^\dagger) H^\dagger (SS^\dagger)^{-1}$. According to A. Mostafazadeh's theorem [60], we can verify that all eigenvalues of H are the same as those of $H_{A=0}$ for the open boundary conditions, giving real values. Furthermore, by utilizing Eq. 19, we can find the following relations:

$$|\Psi_E^R\rangle = \sum_n C_n^E |\Psi_n^R\rangle = \sum_n |\Psi_n^R\rangle \langle \Psi_n | \Psi_E^0 \rangle = S |\Psi_E^0\rangle, \quad (27a)$$

$$\langle \Psi_E^L | = \sum_n (C_n^E)^* \langle \Psi_n^L | = \sum_n \langle \Psi_E^0 | \Psi_n \rangle \langle \Psi_n^L | = \langle \Psi_E^0 | S^{-1}. \quad (27b)$$

We conclude that right (left) eigenstates for finite A can be obtained using the similarity transformation from orthonormal eigenstates of $H_{A=0}$ with respect to the invertible linear operator S (S^{-1}) under open boundary conditions.

NON-HERMITIAN SKIN EFFECT

As proven in previous subsection, for open boundary conditions, the right eigenstates of H can be always obtained by the similarity transformation from orthonormal eigenstates of $H_{A=0}$ with respect to the linear operator $S = \sum_n |\Psi_n^R\rangle \langle \Psi_n| = \sum_n e^{A \sum_j^N l_{nj}} |\Psi_n\rangle \langle \Psi_n|$. For the reason, the coefficients of right eigenstates with respect to the n th orthonormal basis state $|\Psi_n\rangle$ grow exponentially due to the non-orthonormal factor $e^{A \sum_j^N l_{nj}}$ when the magnitude of the imaginary vector potential A increases. In one-particle system, it leads to the exponential localization of all eigenstates at a specific boundary. This phenomena is commonly known as the non-Hermitian skin effect [16, 17]. In many-fermion systems, however, the localization of fermions is influenced not only by the exponential factor of eigenstates but also by the fermionic statistics governed by the Pauli exclusion principle. This interplay gives rise to the many-body skin effect, which can be characterized by the asymmetry of number distribution over open-boundary chain [53–56]. To examine this effect, we can calculate the number distribution functions of right and left eigenstates using $n_E^R(l) = \langle \Psi_E^R | \sum_\sigma c_{l,\sigma}^\dagger c_{l,\sigma} | \Psi_E^R \rangle / \langle \Psi_E^R | \Psi_E^R \rangle$ and $n_E^L(l) = \langle \Psi_E^L | \sum_\sigma c_{l,\sigma}^\dagger c_{l,\sigma} | \Psi_E^L \rangle / \langle \Psi_E^L | \Psi_E^L \rangle$, respectively. The asymmetric distribution leads to an imbalance in the total number of fermions located below $L/2$ ($0 \leq l < L/2$) and above $L/2$ ($L/2 \leq l < L$) sites, which can be quantified by the following formula:

$$\mathcal{I}_E^R = \sum_{L/2 \leq l < L} n_E^R(l) - \sum_{0 \leq l < L/2} n_E^R(l). \quad (28a)$$

$$\mathcal{I}_E^L = \sum_{L/2 \leq l < L} n_E^L(l) - \sum_{0 \leq l < L/2} n_E^L(l). \quad (28b)$$

Non-zero values of \mathcal{I}_E^R (\mathcal{I}_E^L) provides the characteristic feature of the many-body skin effect as determined in right (left) eigenstates.

In the half-filled case ($N = L$), the non-orthonormal factor $e^{A \sum_j^N l_j}$ can be expressed as

$$e^{A \sum_j^N l_j} = e^{A \sum_{l=0}^{L-1} l} e^{A \sum_{l=0}^{L-1} l (\delta_{n_{l,2}} - \delta_{n_{l,0}})} = e^{A \frac{L(L-1)}{2}} e^{A \sum_{l=0}^{L-1} l (\delta_{n_{l,2}} - \delta_{n_{l,0}})}, \quad (29)$$

where n_l refers to the number of fermions occupied at the l th site. Here, $\delta_{n_{l,2}} = 1$ and $\delta_{n_{l,0}} = 1$ indicate the presence of doublon and holon at the l th site, respectively, and the total number of doublons ($N_d = \sum_{l=0}^{L-1} \delta_{n_{l,2}}$) and holons ($N_h = \sum_{l=0}^{L-1} \delta_{n_{l,0}}$) are equal. For states with no doublon-holon pair ($N_d = N_h = 0$), their non-orthonormal factor reaches its minimum with a constant value of $e^{A \frac{L(L-1)}{2}}$. In this case, the skin effect is not involved. In contrast, states with finite doublons and holons exhibit a varying non-orthonormal factor depending on the distribution of doublons and holons. The larger the segregation between doublons and holons, the greater the non-orthonormal factor becomes. Consequently, the many-body skin effect in the half-filled case is characterized by the segregation of doublons and holes.

EFFECTIVE HAMILTONIAN IN STRONG COUPLING LIMIT

In case of strong coupling limit ($U \gg t$), the dominant contribution to energy arises from $H_U = U \sum_{l=0}^{L-1} n_{l,\uparrow} n_{l,\downarrow}$, while the inclusion of $H_t = -t \sum_{l=0}^{L-1} \sum_{\sigma} \left(e^A c_{l+1,\sigma}^\dagger c_{l,\sigma} + e^{-A} c_{l,\sigma}^\dagger c_{l+1,\sigma} \right)$ leads to perturbation energy shifts. Let \mathcal{H}_{N_d} represent a subspace with a fixed number of doublons, N_d . In the second-order perturbation theory, the Hamiltonian can be described using the effective Hamiltonian within \mathcal{H}_{N_d} as follows:

$$H_{N_d} = N_d U + \mathcal{P}_{N_d} H_t \mathcal{P}_{N_d} + \sum_{N'_d (N'_d \neq N_d)} \frac{\mathcal{P}_{N_d} H_t \mathcal{P}_{N'_d} H_t \mathcal{P}_{N_d}}{(N_d - N'_d) U}, \quad (30)$$

where \mathcal{P}_{N_d} is a projection operator onto the subspace $\mathcal{H}_{N_d} N_d$ [63]. First, second, and third terms correspond to the center of energy of the subspace, the kinetic energy contribution within the subspace, and the energy gain resulting from virtual hopping processes that connect different subspaces. In the half-filled case, where the second term becomes zero, we can derive the following equations:

$$H_0 = -\frac{1}{U} \mathcal{P}_0 H_t \mathcal{P}_1 H_t \mathcal{P}_0, \quad (31a)$$

$$H_{L/2} = \frac{L}{2} U + \frac{1}{U} \mathcal{P}_{L/2} H_t \mathcal{P}_{L/2-1} H_t \mathcal{P}_{L/2}, \quad (31b)$$

where \mathcal{P}_0 , \mathcal{P}_1 , $\mathcal{P}_{L/2-1}$, $\mathcal{P}_{L/2}$ are projection operators onto subspaces \mathcal{H}_0 for no doublon-holon pair, \mathcal{H}_1 for one doublon-holon pair, $\mathcal{H}_{L/2-1}$ for $L/2 - 1$ doublon-holon pairs, and $\mathcal{H}_{L/2}$ for $L/2$ doublon-holon pairs, respectively.

As illustrated in Fig. 1(a)–(d), the perturbation energy gain is exclusively permitted within \mathcal{H}_0 , only when neighboring fermions have opposite spin directions. The effective Hamiltonian between fermions at l th and $(l+1)$ th sites can be deduced as follows:

$$\begin{aligned} H_0^{l,l+1} &= -\frac{2t^2}{U} \left(|\uparrow_l, \downarrow_{l+1}\rangle \langle \uparrow_l, \downarrow_{l+1}| + |\downarrow_l, \uparrow_{l+1}\rangle \langle \downarrow_l, \uparrow_{l+1}| - |\uparrow_l, \downarrow_{l+1}\rangle \langle \downarrow_l, \uparrow_{l+1}| - |\downarrow_l, \uparrow_{l+1}\rangle \langle \uparrow_l, \downarrow_{l+1}| \right) \\ &= \frac{4t^2}{U} \left(\mathbf{S}_l \cdot \mathbf{S}_{l+1} - \frac{1}{4} \mathbf{I} \right). \end{aligned} \quad (32)$$

Here, three spin operators at the l th site are given by: $S_{l,x} = \frac{1}{2} (|\uparrow_l\rangle \langle \downarrow_l| + |\downarrow_l\rangle \langle \uparrow_l|)$, $S_{l,y} = \frac{i}{2} (-|\uparrow_l\rangle \langle \downarrow_l| + |\downarrow_l\rangle \langle \uparrow_l|)$, and $S_{l,z} = \frac{1}{2} (|\uparrow_l\rangle \langle \uparrow_l| - |\downarrow_l\rangle \langle \downarrow_l|)$. In this effective Hamiltonian, the non-reciprocal factor $e^{\pm A}$ cancels out during the hopping process, where a fermion hops back and forth between neighboring sites. This observation supports the stabilization of real eigenvalues within states predominantly characterized by the absence of doublon-holon pairs in strong interaction limit.

To describe the effective Hamiltonian in the subspace $\mathcal{H}_{L/2}$, we introduce the creation (annihilation) operator of a doublon at the l th site denoted as $b_l^\dagger = c_{l,\uparrow}^\dagger c_{l,\downarrow}^\dagger$ ($b_l = c_{l,\downarrow} c_{l,\uparrow}$). We can easily verify following commutation relations : $[b_l, b_{l'}^\dagger] = \delta_{l,l'}$, $[b_l, b_{l'}] = [b_l^\dagger, b_{l'}^\dagger] = 0$, and $b_l^\dagger b_l (1 - b_l^\dagger b_l) = 0$. As a result, the doublon can be treated as a hard-core boson. Moreover, the perturbation energy gain is feasible when doublon-holon pairs are located at neighboring sites as illustrated in Figs. 1(e)–(h). We can formulate the effective Hamiltonian between the l th and $(l+1)$ th sites employing the hard-core boson representation:

$$\begin{aligned} H_{L/2}^{l,l+1} &= \frac{2t^2}{U} \left[b_l^\dagger b_l (1 - b_{l+1}^\dagger b_{l+1}) + b_{l+1}^\dagger b_{l+1} (1 - b_l^\dagger b_l) + e^{2A} b_{l+1}^\dagger b_l + e^{-2A} b_l^\dagger b_{l+1} \right] \\ &= \frac{2t^2}{U} \left(e^{2A} b_{l+1}^\dagger b_l + e^{-2A} b_l^\dagger b_{l+1} \right) - \frac{4t^2}{U} b_l^\dagger b_l b_{l+1}^\dagger b_{l+1} + \frac{2t^2}{U} (b_l^\dagger b_l + b_{l+1}^\dagger b_{l+1}). \end{aligned} \quad (33)$$

Thus, we arrive at the effective Hamiltonians within \mathcal{H}_0 and $\mathcal{H}_{L/2}$ as follows:

$$H_0 = J \sum_l \mathbf{S}_l \cdot \mathbf{S}_{l+1} - \frac{J}{4} L, \quad (34a)$$

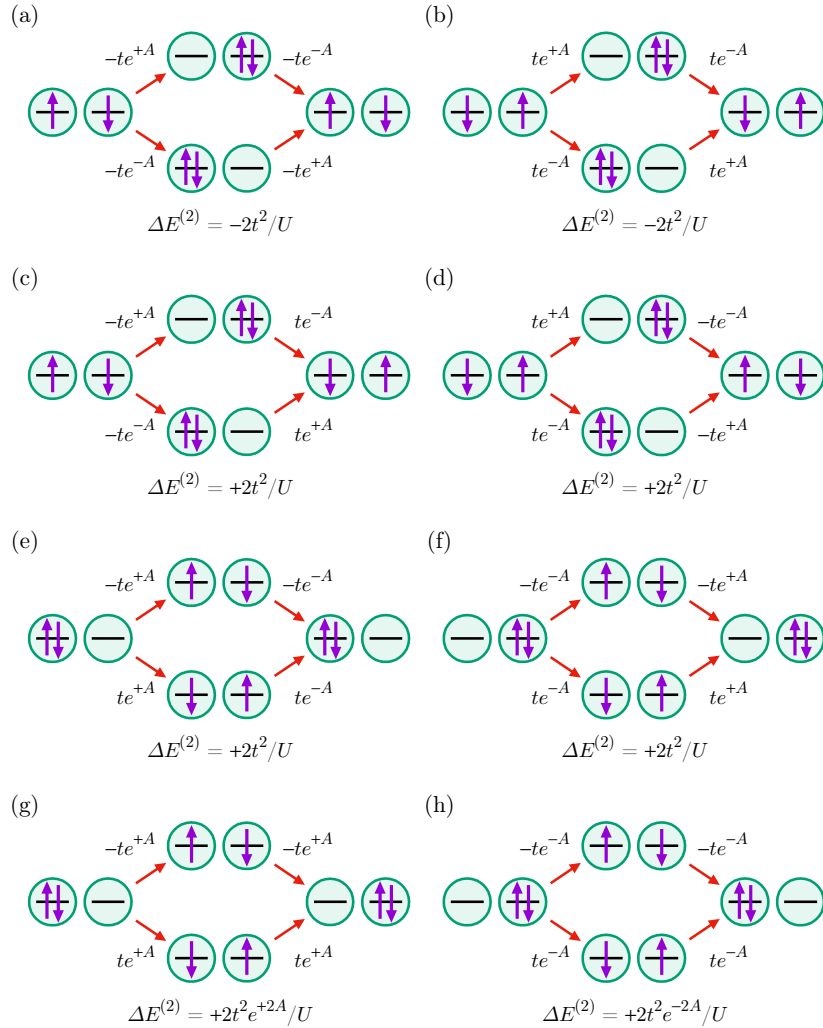


FIG. 1. Schematic diagrams of relevant virtual hopping processes to lead to the perturbation energy gain in the second-order perturbations. Diagrams in (a)–(d) present the virtual hopping processes for the magnetic interactions between neighboring spins in the subspace \mathcal{H}_0 , while diagrams in (e)–(f) describe the virtual hopping processes for the perturbation energies between neighboring doublon-holon pairs in the subspace $\mathcal{H}_{L/2}$. $\Delta E^{(2)}$ below the diagram refers to the energy gain from the virtual hopping process. Let the states for configurations depicted in the left, right, and middle column of the diagrams be $|\Psi_l\rangle$, $|\Psi_r\rangle$, and $|\Psi_m\rangle$, respectively. $\Delta E^{(2)} = \pm \frac{1}{U} \sum_m \langle \Psi_l | H_t | \Psi_m \rangle \langle \Psi_m | H_t | \Psi_r \rangle$, where negative (positive) sign for \mathcal{H}_0 ($\mathcal{H}_{L/2}$).

$$H_{L/2} = T_{\text{eff}} \sum_l \left(e^{A_{\text{eff}}} b_{l+1}^\dagger b_l + e^{-A_{\text{eff}}} b_l^\dagger b_{l+1} \right) + U_{\text{eff}} \sum_l b_l^\dagger b_l b_{l+1}^\dagger b_{l+1} + \frac{L}{2} (U - U_{\text{eff}}), \quad (34b)$$

where $J = \frac{4t^2}{U}$, $T_{\text{eff}} = \frac{2t^2}{U}$, $A_{\text{eff}} = 2A$, and $U_{\text{eff}} = -\frac{4t^2}{U}$, respectively. Hence, $H_{L/2}$ can be regarded as the Hamiltonian of half-filled hard-core bosons. Here, adjacent hard-core bosons are attractively interacted by $U_{\text{eff}} = -\frac{4t^2}{U} < 0$ and their non-reciprocal hopping is given by the effective hopping strength $T_{\text{eff}} = \frac{2t^2}{U}$ and the effective imaginary vector potential $A_{\text{eff}} = 2A$.

EIGENSPECTRUM AT $U = 0$

Figures 2 and 3 depict the asymmetric number density and eigenspectra of the non-interacting case, respectively.

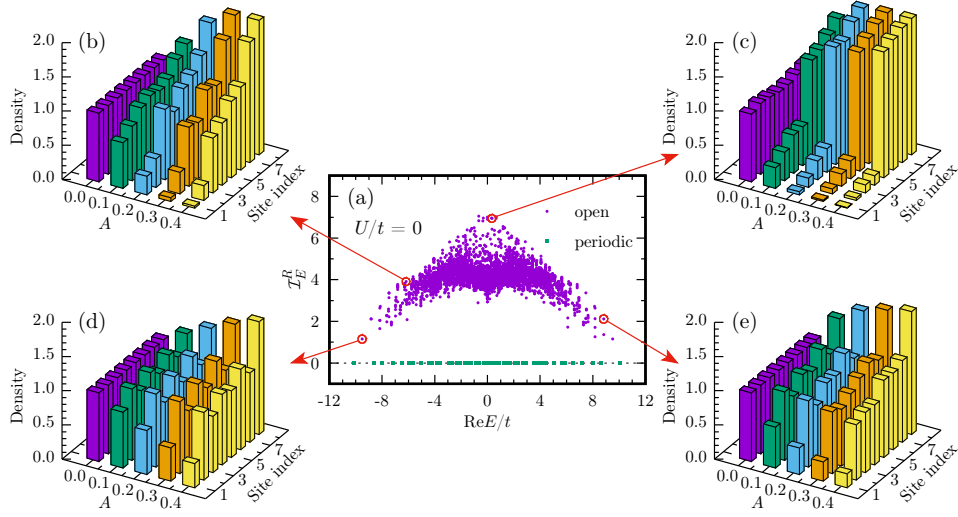


FIG. 2. (a) The number density imbalance in the half-filled Hatano-Nelson model of spin-half fermions ($A = 0.3$) for both open and periodic boundary conditions when $U/t = 0$. The imbalance \mathcal{I}_E^R is calculated by $\sum_{L/2 \leq l < L} n_E^R(l) - \sum_{0 \leq l < L/2} n_E^R(l)$, where $n_E^R(l)$ is the number density of right eigenvalues at the l th site. (b)–(e) the number density distributions as a function of imaginary gauge potential A for specific right eigenstates indicated by red arrows pairs play a dominant role, respectively, for the open boundary condition. All results are obtained for the lattice size of eight ($L = 8$).

ORTHONORMALITY PROPERTY AT THE TOPOLOGICAL TRANSITIONS

We investigate the orthonormality properties of the eigenpairs involved in topological transitions by calculating the overlap between two right eigenstates of the eigenpair as follows:

$$O_{nm}^R = \frac{\langle \Psi_n^R | \Psi_m^R \rangle \langle \Psi_m^R | \Psi_n^R \rangle}{\langle \Psi_n^R | \Psi_n^R \rangle \langle \Psi_m^R | \Psi_m^R \rangle}, \quad (35)$$

where n and m are indices of right eigenvalues of the eigenpair.

In the case of $U = 0$, the Hamiltonian is normal, resulting in all eigenstates being mutually orthonormal. For the reason, the overlap of all eigenpairs becomes to zero as shown in Fig. 4. However, when U has finite values, this orthonormality no longer holds. The overlap takes on finite values, and eventually reaches one at the topological transition point. This point is characterized by the merging of complex conjugate eigenvalues onto the real axis. Thus, two eigenstates of the eigenpair collapse into a singular state at the transition point, which are indeed the exceptional points. Following the transition point, the overlap progressively decreases. As U approaches infinity, the overlaps converge into zero because the Hermiticity is restored.

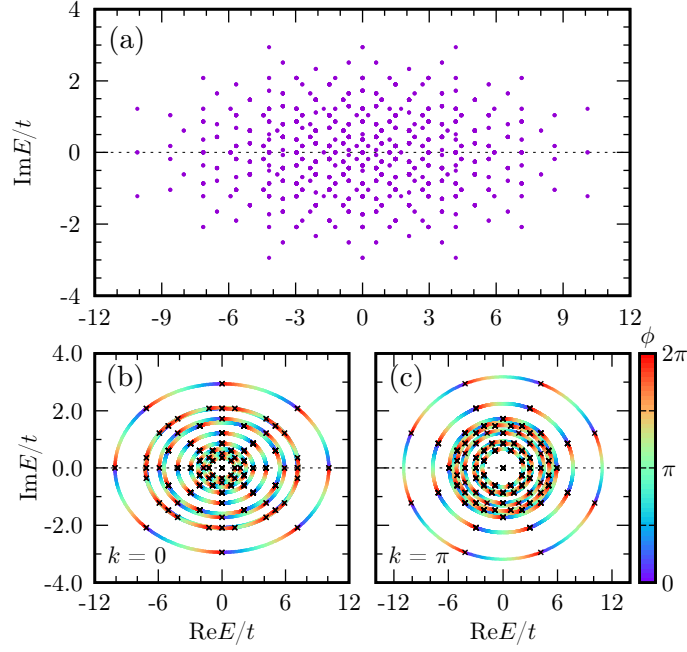


FIG. 3. (a) Spectral distribution of eigenvalues in the half-filled Hatano-Nelson model of spin-half fermions when $U/t = 0$ and $A = 0.3$. Spectral change of eigenvalues as functions of the gauge flux ϕ for the twisted boundary condition in (b) $k = 0$, $S_z = 0$ and (c) $k = \pi$, $S_z = 0$. Here, k is the crystal momentum of one dimensional lattice and S_z is the z -component of the total spin. Cross points refer to the eigenvalues for $\phi = 0$. Spectral data well depict the point-gap topology of complex eigenvalues. Point gap is located at the origin of complex plane. All results are obtained for the lattice size of eight ($L = 8$).

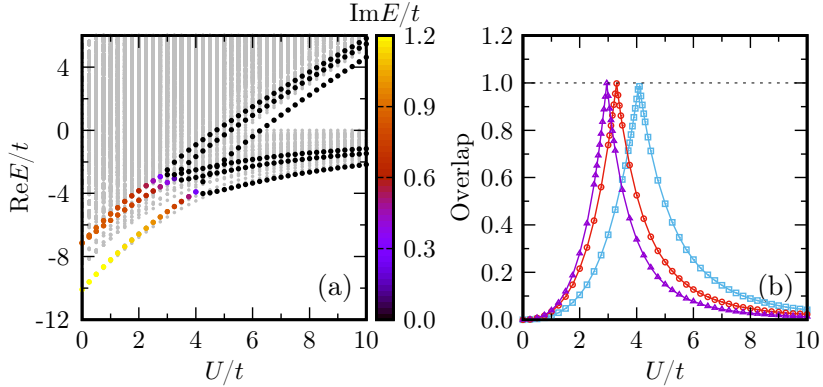


FIG. 4. (a) Real components of eigenvalues as a function of Coulomb repulsion U for $0 \leq U/t \leq 10$. Three examples of the topological transitions are highlighted by the color map. (b) Overlap between two eigenstates involved in the topological transitions. All results are obtained when $A = 0.3$ and $L = 8$.

TOPOLOGICAL TRANSITIONS UNDER AN IMAGINARY GAUGE FLUX

In the absence of an imaginary gauge flux ($A = 0$), the Hamiltonian retains its Hermiticity. This leads to purely real eigenvalues and full orthonormality of eigenstates. When the magnitude of A is large enough, however, eigenvalues are able to form complex conjugate pairs, and the orthonormality among eigenstates is broken. Therefore, we can conjecture that the topological transitions among eigenpairs, which are characterized by the existence of exceptional points, take place by varying the magnitude of A .

Figure 5 presents well these topological transitions in Mott insulating systems with $U/t = 10$. It is reminiscent of the breakdown of the Mott insulator under an imaginary gauge flux [18]. At this transition point, two real eigenvalues coalesce: one in the zero-doublon-holon sector and the other in the one-doublon-holon sector. Subsequently, eigenvalues branch out into complex conjugate pairs. Because the transition occurs at the exceptional point, the

overlap between the eigenpair becomes one at the transition point. These observed behaviors collectively support that the \mathcal{PT} -like transitions, mediated by the imaginary gauge flux A , occur through the exceptional points.

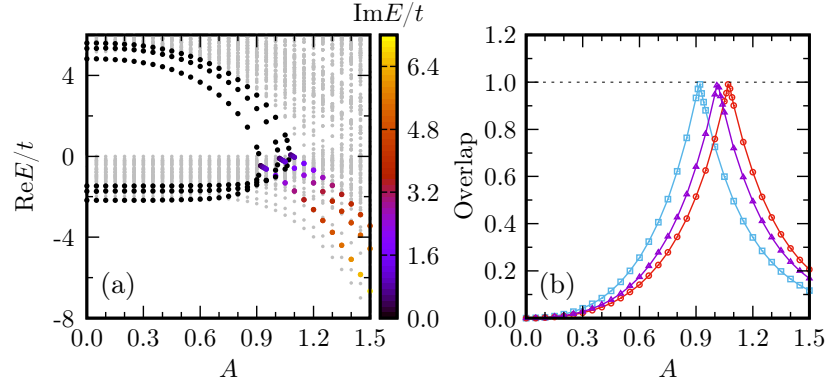


FIG. 5. (a) Real components of eigenvalues as a function of imaginary gauge flux A for $0 \leq A \leq 1.5$. Three examples of the topological transitions are highlighted by the color map. (b) Overlap between two eigenstates involved in the topological transitions. All results are obtained when $U/t = 10$ and $L = 8$.